Materials Advances

ROYAL SOCIETY OF CHEMISTRY

PAPER

View Article Online
View Journal | View Issue

Cite this: *Mater. Adv.*, 2021, 2, 6684

Electron-withdrawing group modified carbazolophane donors for deep blue thermally activated delayed fluorescence OLEDs†

Abhishek Kumar Gupta, ‡[ab] Zhen Zhang,‡[c] Eduard Spuling,[ac] Maria Kaczmarek,[c] Yichuan Wang,[c] Zahid Hassan,[c] Ifor D. W. Samuel,*[b] Stefan Bräse*[cd] and Eli Zysman-Colman*[a]

Received 17th August 2021,
Accepted 2nd September 2021

DOI: 10.1039/d1ma00738f

rsc.li/materials-advances

We report two blue-emitting thermally activated delayed fluorescence (TADF) compounds employing a substituted carbazolophane (Czp) donor (indolo[2.2]paracyclophane). The compounds **CNCzpPhTRZ** and **CF$_3$CzpPhTRZ** show emission maxima of 426 nm and 432 nm, respectively, with high photoluminescence quantum yields (Φ_{PL}) of 73% and 80%, respectively. The singlet–triplet energy gap (ΔE_{ST}) of both emitters is 0.22 eV, resulting in long-delayed lifetimes of 132 μs for **CNCzpPhTRZ** and 158 μs for **CF$_3$CzpPhTRZ** in PPT as the host matrix. Blue organic light-emitting diodes (OLEDs) showed maximum external quantum efficiencies (EQEs) of 7.4% for **CNCzpPhTRZ** and 11.6% for **CF$_3$CzpPhTRZ** with electroluminescence maxima of *ca.* 460 nm.

Introduction

The development of purely organic thermally activated delayed fluorescence (TADF) emitters is considered as one of the most promising approaches to utilize singlet and triplet excitons to access highly efficient organic light-emitting diodes (OLEDs).[1–4] The design principle of generating a structure with spatially separated donor and acceptor moieties to limit the exchange integral between the highest occupied molecular orbital (HOMO) and the lowest unoccupied molecular orbital (LUMO) thereby leading to a small singlet and triplet excited state energy difference, ΔE_{ST}, has been a reliable and fruitful strategy to construct TADF emitters. To obtain a small ΔE_{ST}, there are at present at least six design strategies, which are twisted donor–acceptor,[1] multi-resonance,[5] spiro-conjugation,[6] exciplex,[7] excited-state intramolecular proton transfer (ESIPT)[8] and through space-conjugation.[9] The most popular of these is to electronically decouple the donor and acceptor by ensuring a highly twisted conformation.

The [2.2]paracyclophane (PCP) is a rigid molecule containing two slightly bent benzene rings connected by ethylene bridges. Due to the spatial stacked configuration and a short distance of 2.78–3.09 Å between the two benzene decks, which is smaller than the van der Waals distance between the layers of graphite (3.35 Å), a strong transannular electronic communication can take place, as demonstrated by Bazan *et al.*[10–14] Substituted PCPs can possess planar charity and emissive analogs can exhibit circularly polarized luminescence (CPL).[15] The characteristics of rigid skeleton, chemical and photo stability, planar charity, and through-space electronic communication possessed by the PCP core make it a potentially useful building block for organic semiconductor materials.

In 2018, we first demonstrated that the PCP moiety could be used to mediate weak electronic communication between donor and acceptor groups on different decks of the PCP.[9] ***Trans*-Bz-PCP-TPA** and ***cis*-Bz-PCP-TPA** showed photoluminescence maxima, λ_{PL}, at 455 nm, photoluminescence quantum yields, Φ_{PL}, of 60% (in toluene), ΔE_{ST} = 0.19 eV and delayed lifetime, τ_d, of 3.6 μs for ***trans*-Bz-PCP-TPA** and λ_{PL} of 492 nm, Φ_{PL} of 45% (in toluene), ΔE_{ST} = 0.04 eV and τ_d of 1.8 μs for ***cis*-Bz-PCP-TPA** in 15 wt% mCP doped film (Fig. 1). Zhao *et al.* also reported a series of structurally similar chiral green TADF molecules ***g*-BNMe-Cp** and ***m*-BNMe-Cp** containing a PCP, with emission at 531 nm (Φ_{PL} = 72% in cyclohexane, ΔE_{ST} = 0.17 eV

[a] *Organic Semiconductor Centre, EaStCHEM School of Chemistry, University of St Andrews, St Andrews, Fife, KY16 9ST, UK. E-mail: eli.zysman-colman@st-andrews.ac.uk*
[b] *Organic Semiconductor Centre, SUPA, School of Physics and Astronomy, University of St Andrews, North Haugh, St Andrews, KY16 9SS, UK. E-mail: idws@st-andrews.ac.uk*
[c] *Institute of Organic Chemistry, Karlsruhe Institute of Technology (KIT), Fritz-Haber-Weg 6, 76131, Karlsruhe, Germany. E-mail: braese@kit.edu*
[d] *Institute of Biological and Chemical Systems – Functional Molecular Systems (IBCS-FMS), Karlsruhe Institute of Technology (KIT), Hermann-von-Helmholtz-Platz 1, D-76344, Eggenstein-Leopoldshafen, Germany*

† Electronic supplementary information (ESI) available: The research data supporting this publication can be accessed at DOI: 10.17630/8cbdf064-a1c6-482f-bf7e-77d93ccf516f. See DOI: 10.1039/d1ma00738f

‡ Abhishek Kumar Gupta and Zhen Zhang contributed equally to this work.

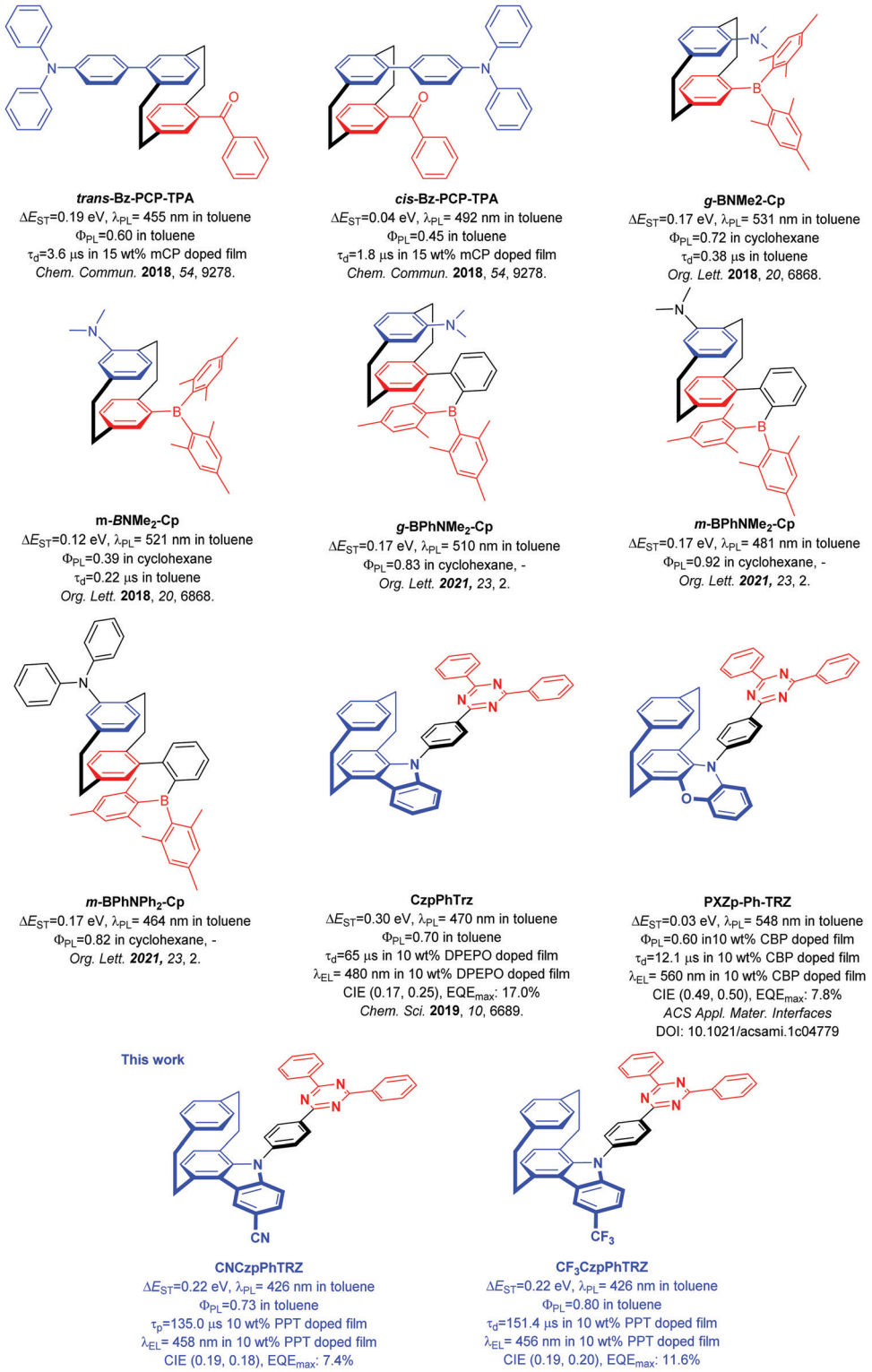

Fig. 1 Chemical structures and performance of PCP-based TADF molecules.

and τ_d = 0.38 μs in toluene) and 521 nm (Φ_{PL} = 39% in cyclohexane, ΔE_{ST} = 0.12 eV and τ_d = 0.22 μs in toluene), respectively (Fig. 1).[16] Recently, the same group introduced a phenylene spacer between the PCP and the acceptor moiety to obtain sky-blue to green TADF emitters showing increased Φ_{PL} (in cyclohexane) to 83% for ***g*-BPhNMe$_2$-Cp**, 93% for ***m*-BPhNMe$_2$-Cp**, and 82% for ***g*-BPhNPh$_2$-Cp** (Fig. 1).[17] Besides using the PCP as a bridge motif to enable electronic coupling between donor and acceptor groups, we also demonstrated how the PCP skeleton could be incorporated within the carbazole donor unit. Carbazolophane

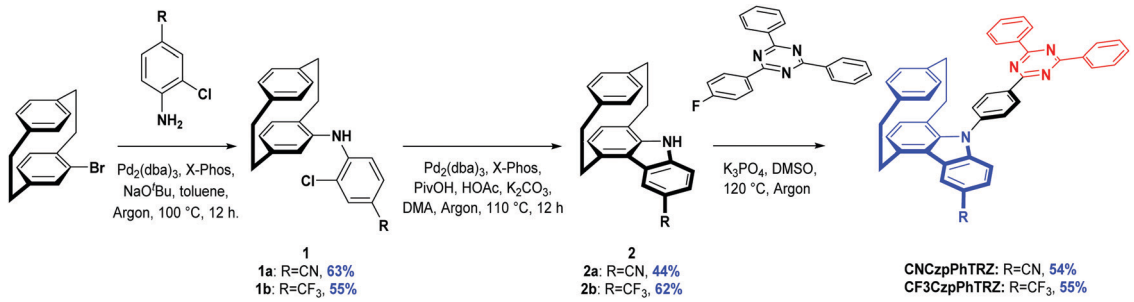

1
1a: R=CN, 63%
1b: R=CF_3, 55%

2
2a: R=CN, 44%
2b: R=CF_3, 62%

CNCzpPhTRZ: R=CN, 54%
CF3CzpPhTRZ: R=CF_3, 55%

Scheme 1 Synthetic route to **CNCzpPhTRZ** and **CF_3CzpPhTRZ**.

(**Czp**, [2]paracyclo[2](1,4)carbazolophane) group is a stronger electron donor that adopts a more twisted conformation due to its greater steric bulk.[9] We reported the chiral TADF emitter **CzpPhTRZ**, which showed a small ΔE_{ST} of 0.16 eV, and λ_{PL} at 482 nm with Φ_{PL} = 69% and a τ_d of 65 μs in 10 wt% DPEPO doped film.[18] Sky-blue OLEDs with **CzpPhTRZ** showed a maximum external quantum efficiency (EQE_{max}) of 17.0% and CIE coordinates of (0.17, 0.25). Zheng and co-workers reported an analog of **CzpPhTRZ**, **PXZp-Ph-TRZ**, where the **Czp** donor was replaced with a phenoxazinephane (**PXZp**). **PXZp-Ph-TRZ** possesses a ΔE_{ST} of 0.03 eV and shows yellow emission with λ_{PL} at 560 nm in 10 wt% CBP doped film. The OLED showed an EQE_{max} of 7.8% and CIE coordinates of (0.49, 0.50).[19] As we can see from Fig. 1 since our first report, a handful of emitters have been reported containing the PCP moiety; however none to date show pure blue emission.

Building on our prior work and with the goal to obtain a blue-shifted emission, we designed two new TADF emitters **CNCzpPhTRZ** and **CF_3CzpPhTRZ**, by introducing electron-withdrawing groups on the **Czp** donor unit of the parent **CzpPhTRZ** emitter. We successfully blue-shifted the emission without adversely affecting the TADF efficiency. **CNCzpPhTRZ** emits at 426 nm, and **CF_3CzpPhTRZ** emits at 432 nm in toluene, representing a *ca.* 40 nm blue-shift compared to that of **CzpPhTRZ**. The Φ_{PL} remained high at 73% and 80%, respectively. Further, we fabricated bluer OLEDs with electroluminescence maxima at *ca.* 460 nm. However, we observed the evolution of a red emission band at around 600 nm in the OLEDs due to degradation of both blue emitters during the operation of the device.

Results and discussion

Synthesis and thermal stability

The synthesis is based on our previously reported route and shown in Scheme 1. Aniline derivatives were coupled to bromo[2.2]paracyclophane with yields of 63% for **1a**, and 55% for **1b**. The generated intermediates were used to form the functionalized carbazolophane donor units with yields of 44% for **2a** and 62% for **2b** *via* a Pd-catalyzed intramolecular oxidative cyclization process where the *ortho*-chlorine atoms act as the directing group. Lastly, the prepared donor **2** and triazine-based acceptor were linked together *via* a nucleophilic aromatic substitution with yields above 50% using tripotassium phosphate as a base in DMSO at 120 °C. The targeted compounds, **CNCzpPhTRZ** and **CF_3CzpPhTRZ**, show strong blue luminescence under UV excitation. The identity and purity of **CNCzpPhTRZ** and **CF_3CzpPhTRZ** were determined by a combination of NMR, MS, HRMS, Mp, HPLC and IR.

Differential scanning calorimetry (DSC) and thermogravimetric analysis (TGA) were carried out to explore the thermal stability of the two emitters (Table 1 and Fig. S2, ESI†). CF_3CzpPhTRZ shows a glass transition temperature (T_g) of 151 °C and 5% weight loss temperature (T_{d5}) of 360 °C. The T_g and T_{d5} of CNCzpPhTRZ are higher than those of CF_3CzpPhTRZ (T_g = 184 °C and T_{d5} = 412 °C).

Theoretical calculations

Density functional theory (DFT) calculations were performed to investigate the frontier orbital densities and energy states of model compounds of the two emitters. The geometries in the ground state of the two emitters were optimized in the gas phase at the PBE0/6-31G(d,p) level of theory. Time-dependent DFT calculations using the Tamm–Dancoff approximation (TDA-DFT) in the gas phase based on the optimized molecular structures provide insight into the energies and nature of the lowest-lying singlet and triplet excited states.[20] The frontier orbitals and energy levels of these molecules are shown in Fig. 2 and Table S1 (ESI†).

Table 1 Electrochemical data, HOMO–LUMO, ΔE_{ST} and thermal stability data of CF_3CzpPhTRZ and CNCzpPhTRZ

Emitters	E_{ox}[a]/V	E_{red}[a]/V	HOMO[b]/eV	LUMO[b]/eV	E_S/E_T[c]/eV	ΔE_{ST}[d]/eV	T_g; T_{d5}/°C
CF_3CzpPhTRZ	1.30	−1.66	−5.64 (6.05)	−2.68	2.91/2.69	0.22	151; 360
CNCzpPhTRZ	1.34	−1.67	−5.68 (5.93)	−2.67	2.92/2.69	0.23	184; 412

[a] E_{ox} and E_{red} are anodic and cathodic peak potentials, respectively, obtained from DPV using F_c/F_c^+ as the internal reference and referenced *versus* SCE (0.46 V *vs.* SCE) in DCM with 0.1 M $[nBu_4N]PF_6$ as the supporting electrolyte.[21] [b] $E_{HOMO/LUMO} = -(E^{ox}/E^{red} + 4.8)$ eV,[22] where E^{ox} is anodic peak potential and E^{red} is cathodic peak potential calculated from DPV relative to F_c/F_c^+. Value inside parentheses determined by ambient pressure photoemission spectroscopy (APS). [c] Obtained from the onset of the prompt fluorescence (time window: 1 ns–100 ns) and phosphorescence spectra (time window: 1 ms–10 ms) of 10 wt% samples doped in PPT at 77 K. [d] $\Delta E_{ST} = E_S - E_T$.

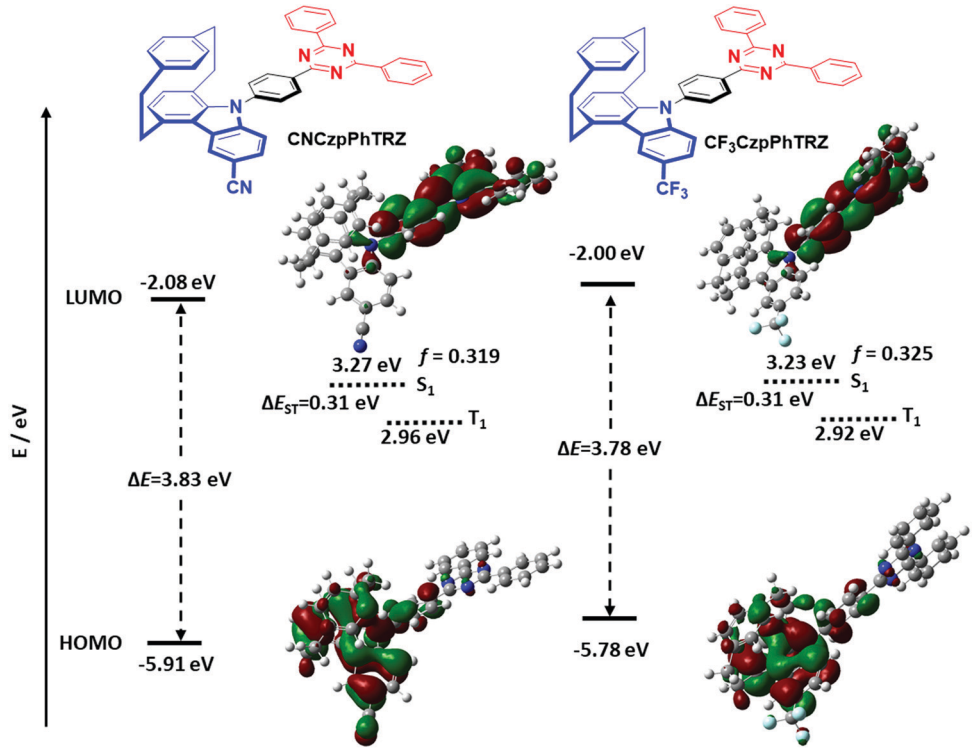

Fig. 2 DFT calculations of **CNCzpPhTRZ** and **CF$_3$CzpPhTRZ**.

The torsion angles between the **Czp** donors and the bridging phenylene are expected not unaffected by the substitution on the distal side of the donor. While for the previously reported **CzpPhTRZ**, the torsion angle obtained from DFT calculations was 58°, the torsion angles for **CF$_3$CzpPhTRZ** and **CNCzpPhTRZ** are 56° and 58°, respectively. The DFT calculations reveal that the frontier orbitals and states are effectively tuned *via* the introduction of electron-withdrawing groups. The HOMO is located primarily on the carbazolophane donor moiety, while the LUMO is distributed across the triazine acceptor and phenylene bridge. The HOMO levels of the two derivatives are expectedly significantly stabilized at −5.91 eV (**CNCzpPhTRZ**), and −5.78 eV (**CF$_3$CzpPhTRZ**) compared to that of the parent emitter **CzpPhTRZ** (−5.54 eV) due to the presence of the electron-withdrawing cyano and trifluoromethyl groups, respectively. The more positive Hammett σ_p value for cyano (0.66) *versus* trifluoromethyl (0.54) explains the 0.13 eV greater stabilization observed for the HOMO of **CNCzpPhTRZ**. The LUMO levels are somewhat less affected by substituting the carbazolophane at −2.08 and −2.00 eV, respectively, for **CNCzpPhTRZ** and **CF$_3$CzpPhTRZ** and deeper than that of **CzpPhTRZ** (−1.88 eV). There is a corresponding increase in the energy of the S_1 state from 3.12 eV (**CzpPhTRZ**) to 3.27 eV (**CNCzpPhTRZ**) and 3.23 eV (**CF$_3$CzpPhTRZ**). The triplet energies are unaffected by the substituents with 2.81 eV (**CzpPhTRZ**), 2.96 eV (**CNCzpPhTRZ**) and 2.92 eV (**CF$_3$CzpPhTRZ**). The ΔE_{ST} values of **CNCzpPhTRZ** (0.31 eV) and **CF$_3$CzpPhTRZ** (0.31 eV) are almost identical to that of **CzpPhTRZ** (0.30 eV), which suggests that these three molecules will be equally promising TADF emitters. The oscillator strengths, *f*, for the transition to the S_1 state of **CNCzpPhTRZ** (f = 0.319) and **CF$_3$CzpPhTRZ** (f = 0.325) are slightly reduced compared to **CzpPhTRZ** (f = 0.418), indicating a slightly slower radiative decay rate.

Electrochemical studies

Cyclic voltammetry (CV) and differential pulse voltammetry (DPV) measurements in dichloromethane (DCM) with tetra-*n*-butylammonium hexafluorophosphate ($TBAPF_6$) as the supporting electrolyte were used to infer the HOMO/LUMO levels of CF$_3$CzpPhTRZ and CNCzpPhTRZ from the redox potentials. The resulting voltammograms are shown in Fig. S1 (ESI†), and the data are summarized in Table 1. Both emitters possess similar irreversible oxidation potentials. The oxidation potential of CF$_3$CzpPhTRZ is 1.30 V *vs.* SCE, and that of CNCzpPhTRZ is 1.34 V *vs.* SCE (Fig. S1, ESI†), which are each assigned to the oxidation of the carbazolophane (Czp) donor moieties, values that are anodically shifted relative to that of CzpPhTRZ (1.14 V).[18] The estimated HOMO levels are −5.64 eV and −5.68 eV for CF$_3$CzpPhTRZ and CNCzpPhTRZ, respectively. These two HOMO levels are very similar, suggesting that the CN and CF$_3$ have a similar electron-withdrawing ability in these compounds.

Further, the ionization potential was directly measured by UV ambient pressure photoemission spectroscopy (APS) and showed deeper levels of 6.05 eV for CF$_3$CzpPhTRZ and 5.93 eV for CNCzpPhTRZ than those determined from the solution-state electrochemistry, this due in part to the different measurement environments (neat film for APS and DCM for DPV). These values align much more closely to the DFT calculated values (*vide supra*), although we note the calculations are *in vacuo* whereas the measurements are on solid films. The reduction

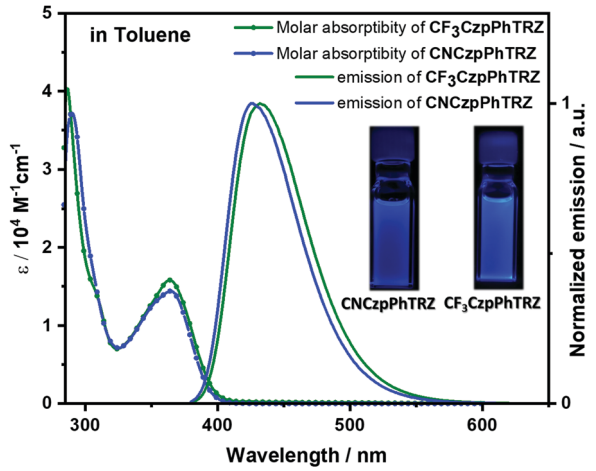

Fig. 3 Molar absorptivity and photoluminescence spectra of **CF_3CzpPhTRZ** and **CNCzpPhTRZ** in toluene at 298 K (λ_{exc} = 360 nm). Inset: photos of photoexcited solutions in toluene.

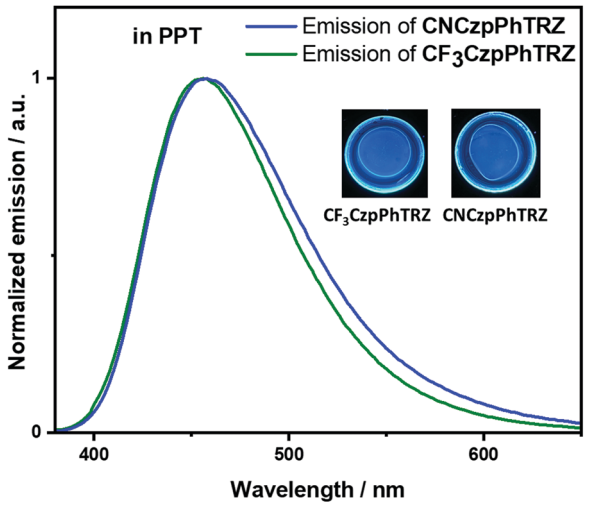

Fig. 4 Photoluminescence spectra of **CF_3CzpPhTRZ** and **CNCzpPhTRZ** dispersed at 10 wt% in PPT matrix at 295 K (λ_{exc} = 360 nm).

waves assigned to the reduction of the cyaphenine acceptor are quasi-reversible at −1.67 V *vs.* SCE. The reduction potentials are slightly shifted anodically compared to E_{red} of −1.78 V for CzpPhTRZ.[18] The corresponding LUMO levels are −2.68 V and −2.67 V for CF_3CzpPhTRZ and CNCzpPhTRZ, respectively.

Solution-state photophysical studies

Both molecules show similar absorption and photoexcitation spectra in dilute toluene (Fig. 3 and Fig. S3, ESI†). The absorption bands of **CF_3CzpPhTRZ** at 363 nm and **CNCzpPhTRZ** at 365 nm are of similar intensities ($\varepsilon = 1.6 \times 10^4$ *vs.* 1.4×10^4 M^{-1} cm^{-1}) and are assigned to an intramolecular charge transfer (ICT) from the carbazolophane donor to the triazine acceptor. These CT bands are *ca.* 10 nm hypsochromically shifted compared to the CT band of the reference compound **CzpPhTRZ**.[18]

The photoluminescence (PL) spectra of both emitters in toluene are shown in Fig. 3. The PL maxima of **CF_3CzpPhTRZ** at 432 nm and **CNCzpPhTRZ** at 426 nm are significantly blue-shifted compared to that of the reference **CzpPhTRZ** emitter (λ_{PL} = 470 nm). The emission spectra are unstructured, indicative of an excited state with a strong ICT character. The full-width-at-half maximum (FWHM) for **CNCzpPhTRZ** (0.36 eV) is slightly smaller than that of **CF_3CzpPhTRZ** (0.41 eV). The PL quantum yield (Φ_{PL}) values in degassed toluene are 80% for **CF_3CzpPhTRZ** and 73% for **CNCzpPhTRZ**, which decreased upon exposure to oxygen to 69% for **CF_3CzpPhTRZ** and 61% for **CNCzpPhTRZ**. The Φ_{PL} of both emitters in toluene is higher than that of the parent emitter (70% in degassed toluene and 55% after exposure to oxygen).[18] Triplets are sensitive to quenching by oxygen and so the lower Φ_{PL} after exposure to oxygen shows that triplets play a role in the light emission process.[23,24] The time-resolved PL decays of both compounds exhibited mono-exponential decay kinetics with PL lifetimes, τ, of 5.47 ns and 4.87 ns for **CF_3CzpPhTRZ** and **CNCzpPhTRZ**, respectively (Fig. S4, ESI†); no delayed emission in toluene was detected despite the oxygen sensitivity noted for the Φ_{PL}. Thus, the delayed fluorescence in **CzpPhTRZ**, **CF_3CzpPhTRZ**, and **CNCzpPhTRZ** in toluene is smaller than we can reliably detect.

Photophysical properties in thin films

Recognizing examples where there is little evidence for TADF in solution but that TADF is prevalent in the solid-state for compounds with relatively large calculated ΔE_{ST} values,[24,26] we next focused our attention on the photophysical properties of **CF_3CzpPhTRZ** and **CNCzpPhTRZ** in doped thin films. Initially, a photophysical investigation was conducted on spin-coated 10 wt% doped films in poly(methyl methacrylate) (PMMA) as the polarity of this host closely mimics that of toluene (PhMe). The absorption bands are of similar energy to those in PhMe, with the CT band observed at about 363 nm (Fig. S5, ESI†). Both compounds showed the unstructured ICT-based emission at around 435 nm, similar to that observed

Table 2 Photophysical properties of **CF_3CzpPhTRZ** and **CNCzpPhTRZ**[a]

Emitters	λ_{PL}/nm	τ_p/ns	τ_d/μs	Φ_{PL}/%
In toluene[b]				
CF_3CzpPhTRZ	432	5.47	—	80 (69)
CNCzpPhTRZ	426	4.87	—	73 (61)
10 wt% doped in PMMA[c]				
CF_3CzpPhTRZ	436	6.84	151.4	63 (61)
CNCzpPhTRZ	435	7.32	132.1	62 (59)
10 wt% doped in PPT[c]				
CF_3CzpPhTRZ	456	6.63	158.3	70 (65)
CNCzpPhTRZ	458	6.75	135.0	65 (60)

[a] At 298 K. [b] Quinine sulfate (0.5 M) in H_2SO_4 (aq.) was used as the reference (Φ_{PL}: 54.6%, λ_{exc} = 360 nm).[25] Values quoted are in degassed solutions, which were prepared by three freeze–pump–thaw cycles. The values in parentheses are in the presence of O_2. [c] Thin films were prepared by spin-coating 10 wt% doped samples in PMMA and PPT. Steady-state and time-resolved emission spectra were recorded at 298 K under an O_2-free atmosphere (λ_{exc} = 360 nm for steady-state and λ_{exc} = 379 nm for time-resolved emission). Photoluminescence quantum yields of thin films were determined using an integrating sphere (λ_{exc} = 300 nm or 360 nm) under N_2 atmosphere at 298 K. The values in parentheses are in the presence of O_2.

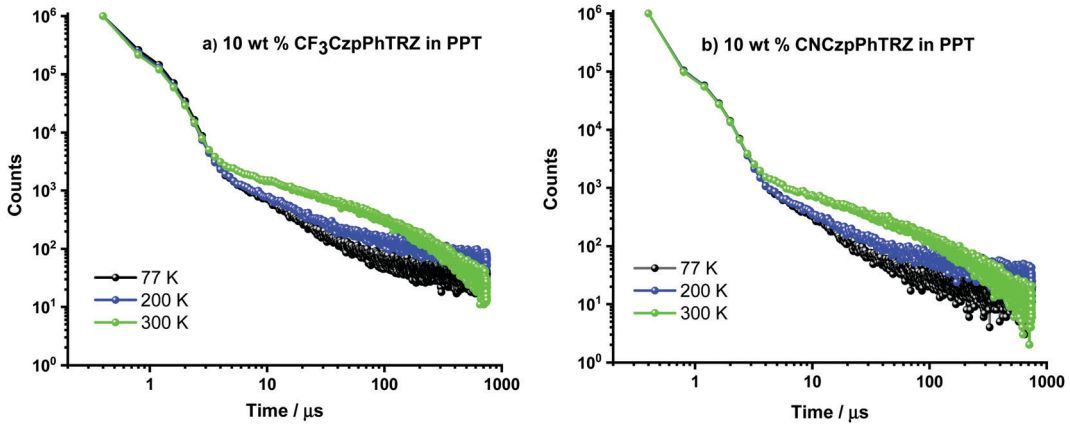

Fig. 5 Temperature-dependent time-resolved photoluminescence lifetime of 10 wt% doped films of (a) CF_3CzpPhTRZ and (b) CNCzpPhTRZ in PPT (λ_{exc} = 379 nm).

in PhMe (Fig. S5, ESI†). The PL spectra are blue-shifted by *ca.* 30 nm compared to that of the parent emitter **CzpPhTRZ**. The Φ_{PL} values are modestly decreased relative to those in solution at 63% and 62% for **CF_3CzpPhTRZ** and **CNCzpPhTRZ**, respectively, under N_2 atmosphere, likely reflective of some aggregation-caused quenching. Biexponential decay kinetics were observed in the time-resolved decays with τ_p values of 6.84 ns and 7.32 ns and τ_d values of 151.4 and 132.1 μs for **CF_3CzpPhTRZ** and **CNCzpPhTRZ**, respectively (Fig. S6, ESI†). We measured prompt fluorescence and phosphorescence spectra of both emitters in PMMA films at 77 K. The energy difference, taken from the onsets of these spectra, provides ΔE_{ST} values of 0.27 and 0.30 eV for **CF_3CzpPhTRZ** and **CNCzpPhTRZ**, respectively. These data are consistent with TADF being operative for the emitters in PMMA films. We then investigated the photophysical behavior of the both compounds in suitably high triplet energy and deep HOMO level OLED-relevant hosts such as bis[2-(diphenylphosphino)phenyl]ether oxide (DPEPO, E_T = 3.0 eV, E_{HOMO} = −6.3 eV)[27,28] and 2,8-bis(diphenyl-phosphoryl)-dibenzo[*b*,*d*]thiophene (PPT, E_T = 3.1 eV, E_{HOMO} = −6.7 eV).[29] A concentration study of both emitters revealed that the Φ_{PL} was highest in 10 wt% doped films in PPT (Table S2, ESI†). The Φ_{PL} of 10 wt% **CF_3CzpPhTRZ** doped in PPT is 70%, while in DPEPO at the same doping concentration, it is 53%. Similarly, the Φ_{PL} of 10 wt% **CNCzpPhTRZ** doped in PPT is 65%, and in the corresponding DPEPO film, it is 52%. By contrast, the parent emitter **CzpPhTRZ** showed Φ_{PL} of 69% in the 10 wt% doped DPEPO film and only 55% in the 10 wt% doped PPT film.[18] The absorption spectra in these host matrices are very similar to those in PMMA (Fig. S7, ESI†). However, λ_{PL} of both emitters are about 20 nm red-shifted at around 456 nm in these two host matrices, suggesting stronger aggregation[30,31] (Fig. 4 and Fig. S8 (ESI†) and Table 2). The emission of both emitters is expectedly blue-shifted (∼25 nm) in comparison to parent emitter **CzpPhTRZ** (λ_{PL} = 482 nm in 10 wt% doped films in DPEPO).[18] The time-resolved PL decays in PPT show a nanosecond prompt emission and microsecond delayed emission at room temperature with comparable values to those measured in PMMA. The τ_d values of the 10 wt% doped PPT films are 158.3 μs for **CF_3CzpPhTRZ** and 135.0 μs for **CNCzpPhTRZ**, which is significantly longer than that measured for parent emitter **CzpPhTRZ** in the 10 wt% DPEPO film (τ_d = 65 μs). The temperature-dependent time-resolved PL decays in PPT are shown in Fig. 5. The prompt emission is insensitive to temperature, while the delayed emission is thermally activated, a behavior consistent with TADF.

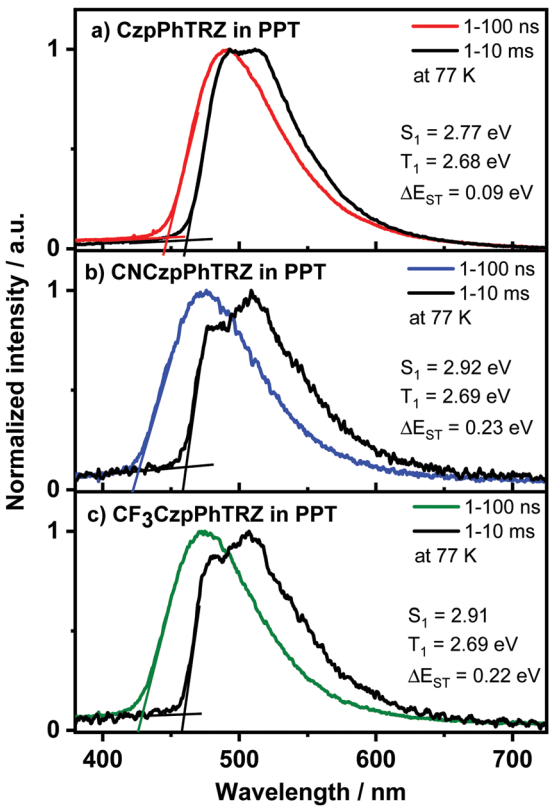

Fig. 6 77 K prompt PL and phosphorescence spectra measurement of 10 wt% (a) **CzpPhTRZ** (b) **CF_3CzpPhTRZ** and (c) **CNCzpPhTRZ** doped in PPT host (λ_{exc} = 343 nm), the ΔE_{ST} value is taken from the onset value difference between the 77 K prompt fluorescence and phosphorescence spectra.

We next prepared 10 wt% doped films of each emitter in PPT as a host matrix. As shown in Fig. 6, the S_1 levels of

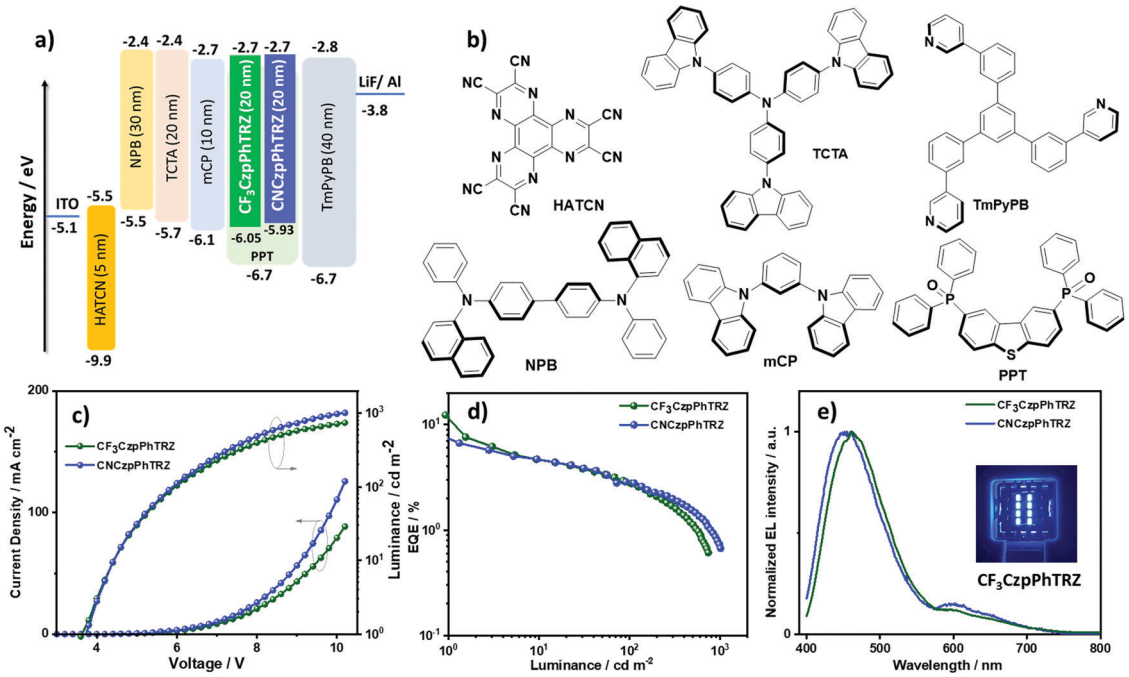

Fig. 7 (a) Energy level diagram of materials employed in the devices; (b) molecular structure of materials used in the devices; (c) current density and luminescence *versus* voltage characteristics for the devices; (d) external quantum efficiency *versus* luminescence curves for the devices; (e) electroluminescence spectra of the device of CF_3CzpPhTRZ and CNCzpPhTRZ, the inset is the electroluminescence of CF_3CzpPhTRZ.

CF_3CzpPhTRZ (S_1 = 2.92 eV) and **CNCzpPhTRZ** (S_1 = 2.91) are very similar and at higher energy than that of the parent emitter **CzpPhTRZ** (S_1 = 2.77 eV); interestingly, the S_1 level of **CzpPhTRZ** in DPEPO is 2.89 eV. The S_1 energies in PPT are only slightly lower in energy than those determined in PMMA (S_1 = 3.0 eV), Fig. S9 (ESI†). The T_1 levels remain largely the same, regardless of the nature of the host medium or the structure of the emitter, and are of similar magnitude to their corresponding triphenyl triazine acceptor segments in toluene,[32] indicating that the T_1 state is locally excited (^{3}LE) character. The T_1 levels for **CF_3CzpPhTRZ**, **CNCzpPhTRZ** and **CzpPhTRZ** are all around 2.69 eV in PPT (Fig. 6) and closely resembles those measured in PMMA at 2.73 eV (Fig. S9, ESI†) and the reported triplet energy of **CzpPhTRZ** in DPEPO (2.73 eV).[18] The corresponding ΔE_{ST} values are 0.22 eV for **CF_3CzpPhTRZ**, 0.23 eV for **CNCzpPhTRZ**, and 0.09 eV for **CzpPhTRZ** in PPT (Fig. 6 and Table 2); the reported ΔE_{ST} of 10 wt% **CzpPhTRZ** doped in DPEPO is 0.16 eV.[18] The larger ΔE_{ST} values for **CF_3CzpPhTRZ** and **CNCzpPhTRZ** explain the longer delayed lifetimes and less efficient RISC, which can be rationalized due to the weaker electron-donor leading to a larger overlap integral.

Device characterization

Based on the promising photophysical properties of **CF_3CzpPhTRZ** and **CNCzpPhTRZ** in PPT films, we fabricated thermally-evaporated multilayer bottom-emitting OLEDs. The OLED stack architecture is shown in Fig. 7a and consisted of: indium tin oxide (ITO)/1,4,5,8,9,11-hexaazatriphenylenehexacarbonitrile (HATCN) (5 nm)/*N*,*N*′-di(1-naphthyl)-*N*,*N*′-diphenyl-(1,1′-biphenyl)-4,4′-diamine (NPB) (30 nm)/tris(4-carbazoyl-9-ylphenyl)amine (TCTA) (20 nm)/1,3-bis(*N*-carbazolyl)benzene (mCP) (10 nm)/emissive layer (20 nm)/1,3,5-tri[(3-pyridyl)-phen-3-yl]benzene (TmPyPB) (40 nm)/LiF (0.5 nm)/Al (100 nm), where HATCN plays the role of hole-injection layer (HIL), NPB and TCTA were employed as hole-transport layer (HTL), mCP acts as an electron/exciton-blocker layer (EBL) and TmPyPB plays the role of an electron-transport layer (ETL) and hole-blocking layer (HBL) due to its deep HOMO (−6.7 eV);[33] LiF acts as electron-injection layer (EIL) by modifying the work function of the aluminum cathode. The molecular structures of the materials used in these OLEDs are shown in Fig. 7b. The emission layer (EML) comprises 10 wt% of **CF_3CzpPhTRZ** or 10 wt% **CNCzpPhTRZ** doped into PPT. The electroluminescence properties of the OLEDs are summarized in Table 3, and current density–voltage–brightness

Table 3 Electroluminescence data for the devices

Emitter	Host	V_{on}[a]/V	λ_{EL}[b]/nm	CE[c]/cd A^{-1}	PE_{max}/lm W^{-1}	EQE[c]/%	CIE[d]/*x*, *y*
CF_3CzpPhTRZ (10 wt%)	PPT	3.7	460	16.8	13.7	11.6/2.7	0.186, 0.200
CNCzpPhTRZ (10 wt%)	PPT	3.7	456	9.1	7.5	7.4/2.7	0.194, 0.182

[a] The turn-on voltage at a brightness 1 cd m^{-2}. [b] The electroluminescence maximum recorded at 6 V. [c] EQE_{max} at 1 cd m^{-2} and EQE at 100 cd m^{-2}. [d] The CIE coordinates were recorded at 7 V.

(*J–V–L*) curves, EQE–luminance curves and electroluminescence spectra (EL) are given in Fig. 7c–e. The turn-on voltage of the devices is *ca.* 3.7 V at 1 cd m^{-2}. The maximum external quantum efficiency (EQE_{max}) of the **CF_3CzpPhTRZ** and **CNCzpPhTRZ** based devices at 1 cd m^{-2} and is 11.6% and 7.4%, respectively, with a current efficiency (CE) = 16.8 cd A^{-1} and 9.08 cd A^{-1} and a power efficiency (PE) = 13.7 lm W^{-1} and 7.5 lm W^{-1}, respectively (Fig. S10 and S11, ESI†). The devices with both emitters show high-efficiency roll-off with EQEs at 100 cd m^{-2} at only 2.7%, due in part to inefficient harvesting triplet exciton because of the high triplet lifetime of both emitters. As expected, the optimized **CF_3CzpPhTRZ** and **CNCzpPhTRZ** based devices display a blue-shifted emission at around 460 nm compared to the previously reported OLED with **CzpPhTRZ** (λ_{EL} = 480 nm), consistent with the trend of their film PL emission (Fig. 7e). The corresponding CIE coordinates are (0.186, 0.200), and (0.194, 0.182) for **CF_3CzpPhTRZ** and **CNCzpPhTRZ**, respectively.

Surprisingly, we observed spectral changes of the electroluminescence in both devices with an emission band in the region of 600 nm developing as the device was run whereas upon photoexcitation, we did not observe any emission around 600 nm. We ascribe this new feature in the EL spectrum to degradation of the emitter during device operation. We also observed emission at around 600 nm from the decomposed residue isolated from the sample boat after gradient sublimation under vacuum, which is very similar to the EL feature above 600 nm (Fig. S12, ESI†) and may be attributed to aggregate formation.[34]

Conclusions

We developed two new TADF emitters containing a substituted carbazolophane (Czp) donor unit (indolo[2.2]paracyclophane) containing the electron-withdrawing groups cyano (**CN**) and trifluoromethyl (**CF_3**) to obtain the deep and pure blue emission. Both emitters show high photoluminescence quantum yield. The ΔE_{ST} is 0.23 eV for **CF_3CzpPhTRZ** and 0.22 eV for **CNCzpPhTRZ** with long-delayed lifetime of 158.3 μs for **CF_3CzpPhTRZ** and 135.0 μs for **CNCzpPhTRZ** in PPT host shows TADF behavior. Blue OLEDs were fabricated with these new TADF emitters showing an EQE_{max} of 7.4% for **CNCzpPhTRZ** and 11.6% for **CF_3CzpPhTRZ** at electroluminescence wavelength around 460 nm with CIE coordinates of (0.194, 0.182) for the device with **CF_3CzpPhTRZ** and (0.186, 0.200) for the device with **CF_3CzpPhTRZ**. We observed an unexpected emission band around 600 nm in OLEDs upon electrical excitation, which we attributed to degradation of the emitter.

Conflicts of interest

There are no conflicts to declare.

Acknowledgements

AKG is grateful to the Royal Society for Newton International Fellowship NF171163. We acknowledge support from the Engineering and Physical Sciences Research Council of the UK (grants EP/P010482/1 and EP/L017008/1). The German Research Foundation (formally Deutsche Forschungsgemeinschaft DFG) in the framework of SFB1176 Cooperative Research Centre ''Molecular Structuring of Soft Matter'' (CRC1176, A4, B3, C2, C6) and the cluster 3D Matter made to order all funded under Germany's Excellence Strategy 2082/1-390761711 are acknowledged for financial contributions.

References

1 H. Uoyama, K. Goushi, K. Shizu, H. Nomura and C. Adachi, Highly efficient organic light-emitting diodes from delayed fluorescence, *Nature*, 2012, **492**(7428), 234–238, DOI: 10.1038/nature11687.
2 Z. Yang, Z. Mao, Z. Xie, Y. Zhang, S. Liu, J. Zhao, J. Xu, Z. Chi and M. P. Aldred, Recent advances in organic thermally activated delayed fluorescence materials, *Chem. Soc. Rev.*, 2017, **46**(3), 915–1016, DOI: 10.1039/c6cs00368k.
3 M. Y. Wong and E. Zysman-Colman, Purely organic thermally activated delayed fluorescence materials for organic light-emitting diodes, *Adv. Mater.*, 2017, **29**(22), 1605444, DOI: 10.1002/adma.201605444.
4 G. Hong, X. Gan, C. Leonhardt, Z. Zhang, J. Seibert, J. M. Busch and S. Bräse, A brief history of OLEDs—emitter development and industry milestones, *Adv. Mater.*, 2021, **33**(9), DOI: 10.1002/adma.202005630.
5 T. Hatakeyama, K. Shiren, K. Nakajima, S. Nomura, S. Nakatsuka, K. Kinoshita, J. Ni, Y. Ono and T. Ikuta, Ultrapure blue thermally activated delayed fluorescence molecules: Efficient HOMO–LUMO separation by the multiple resonance effect, *Adv. Mater.*, 2016, **28**(14), 2777–2781, DOI: 10.1002/adma.201505491.
6 L. Gan, Z. Xu, Z. Wang, B. Li, W. Li, X. Cai, K. Liu, Q. Liang and S. J. Su, Utilizing a spiro TADF moiety as a functional electron donor in TADF molecular design toward efficient ''multichannel'' reverse intersystem crossing, *Adv. Funct. Mater.*, 2019, **29**(20), 1–8, DOI: 10.1002/adfm.201808088.
7 M. Sarma and K. T. Wong, Exciplex: An intermolecular charge-transfer approach for TADF, *ACS Appl. Mater. Interfaces*, 2018, **10**(23), 19279–19304, DOI: 10.1021/acsami.7b18318.
8 A. K. Gupta, W. Li, A. Ruseckas, C. Lian, C. L. Carpenter-Warren, D. B. Cordes, A. M. Z. Slawin, D. Jacquemin, I. D. W. Samuel and E. Zysman-Colman, Thermally activated delayed fluorescence emitters with intramolecular proton transfer for high luminance solution-processed organic light-emitting diodes, *ACS Appl. Mater. Interfaces*, 2021, **13**(13), 15459–15474, DOI: 10.1021/acsami.1c02248.
9 E. Spuling, N. Sharma, I. D. W. Samuel, E. Zysman-Colman and S. Bräse, (Deep) blue through-space conjugated TADF

emitters based on [2.2]paracyclophanes, *Chem. Commun.*, 2018, **54**(67), 9278–9281, DOI: 10.1039/c8cc04594a.

10 Z. Hassan, E. Spuling, D. M. Knoll and S. Bräse, Regioselective functionalization of [2.2]paracyclophanes: Recent synthetic progress and perspectives, *Angew. Chem., Int. Ed.*, 2020, **59**(6), 2156–2170, DOI: 10.1002/anie.201904863.

11 Z. Hassan, E. Spuling, D. M. Knoll, J. Lahann and S. Bräse, Planar Chiral [2.2]Paracyclophanes: From Synthetic Curiosity to Applications in Asymmetric Synthesis and Materials, *Chem. Soc. Rev.*, 2018, **47**(18), 6947–6963, DOI: 10.1039/c7cs00803a.

12 J. Zyss, I. Ledoux, S. Volkov, V. Chernyak, S. Mukamel, G. P. Bartholomew and G. C. Bazan, Through-space charge transfer and nonlinear optical properties of substituted paracyclophane, *J. Am. Chem. Soc.*, 2000, **122**(48), 11956–11962, DOI: 10.1021/ja0022526.

13 A. Marrocchi, I. Tomasi and L. Vaccaro, Organic small molecules for photonics and electronics from the [2.2]paracyclophane scaffold, *Isr. J. Chem.*, 2012, **52**(1–2), 41–52, DOI: 10.1002/ijch.201100091.

14 D. J. Cram and J. M. Cram, Cyclophane chemistry: Bent and battered benzene rings, *Acc. Chem. Res.*, 1971, **4**(6), 204–213, DOI: 10.1021/ar50042a003.

15 Y. Morisaki, M. Gon, T. Sasamori, N. Tokitoh and Y. Chujo, Planar chiral tetrasubstituted [2.2]paracyclophane: Optical resolution and functionalization, *J. Am. Chem. Soc.*, 2014, **136**(9), 3350–3353, DOI: 10.1021/ja412197j.

16 M. Y. Zhang, Z. Y. Li, B. Lu, Y. Wang, Y. D. Ma and C. H. Zhao, Solid-state emissive triarylborane-based [2.2]paracyclophanes displaying circularly polarized luminescence and thermally activated delayed fluorescence, *Org. Lett.*, 2018, **20**(21), 6868–6871, DOI: 10.1021/acs.orglett.8b02995.

17 M. Y. Zhang, X. Liang, D. N. Ni, D. H. Liu, Q. Peng and C. H. Zhao, 2-(Dimesitylboryl)phenyl-substituted [2.2]paracyclophanes featuring intense and sign-invertible circularly polarized luminescence, *Org. Lett.*, 2021, **23**(1), 2–7, DOI: 10.1021/acs.orglett.0c02463.

18 N. Sharma, E. Spuling, C. M. Mattern, W. Li, O. Fuhr, Y. Tsuchiya, C. Adachi, S. Bräse, I. D. W. Samuel and E. Zysman-Colman, Turn on of sky-blue thermally activated delayed fluorescence and circularly polarized luminescence (cpl): *Via* increased torsion by a bulky carbazolophane donor, *Chem. Sci.*, 2019, **10**(27), 6689–6696, DOI: 10.1039/c9sc01821b.

19 C. Liao, Y. Zhang, S. Ye and W. Zheng, Planar chiral [2.2]paracyclophane-based thermally activated delayed fluorescent materials for circularly polarized electroluminescence, *ACS Appl. Mater. Interfaces*, 2021, 1c04779, DOI: 10.1021/acsami.1c04779.

20 M. Moral, L. Muccioli, W. J. Son, Y. Olivier and J. C. Sancho-Garcia, Theoretical rationalization of the singlet–triplet gap in oleds materials: Impact of charge-transfer character, *J. Chem. Theory Comput.*, 2015, **11**(1), 168–177, DOI: 10.1021/ct500957s.

21 N. G. Connelly and W. E. Geiger, Chemical redox agents for organometallic chemistry, *Chem. Rev.*, 1996, **96**(2), 877–910, DOI: 10.1021/cr940053x.

22 C. M. Cardona, W. Li, A. E. Kaifer, D. Stockdale and G. C. Bazan, Electrochemical considerations for determining absolute frontier orbital energy levels of conjugated polymers for solar cell applications, *Adv. Mater.*, 2011, **23**(20), 2367–2371, DOI: 10.1002/adma.201004554.

23 H. Tanaka, K. Shizu, H. Miyazaki and C. Adachi, Efficient green thermally activated delayed fluorescence (TADF) from a phenoxazine–triphenyltriazine (PXZ–TRZ) derivative, *Chem. Commun.*, 2012, **48**(93), 11392–11394, DOI: 10.1039/c2cc36237f.

24 M. Y. Wong, S. Krotkus, G. Copley, W. Li, C. Murawski, D. Hall, G. J. Hedley, M. Jaricot, D. B. Cordes, A. M. Z. Slawin, Y. Olivier, D. Beljonne, L. Muccioli, M. Moral, J. C. Sancho-Garcia, M. C. Gather, I. D. W. Samuel and E. Zysman-Colman, Deep-blue oxadiazole-containing thermally activated delayed fluorescence emitters for organic light-emitting diodes, *ACS Appl. Mater. Interfaces*, 2018, **10**(39), 33360–33372, DOI: 10.1021/acsami.8b11136.

25 A. M. Brouwer, Standards for photoluminescence quantum yield measurements in solution (IUPAC Technical Report), *Pure Appl. Chem.*, 2011, **83**(12), 2213–2228, DOI: 10.1351/PAC-REP-10-09-31.

26 W. Li, Z. Li, C. Si, M. Y. Wong, K. Jinnai, A. K. Gupta, R. Kabe, C. Adachi, W. Huang, E. Zysman-Colman and I. D. W. Samuel, Organic long-persistent luminescence from a thermally activated delayed fluorescence compound, *Adv. Mater.*, 2020, **32**(45), 1–9, DOI: 10.1002/adma.202003911.

27 Q. Zhang, T. Komino, S. Huang, S. Matsunami, K. Goushi and C. Adachi, Triplet exciton confinement in green organic light-emitting diodes containing luminescent charge-transfer Cu(I) complexes, *Adv. Funct. Mater.*, 2012, **22**(11), 2327–2336, DOI: 10.1002/adfm.201101907.

28 C. Han, Y. Zhao, H. Xu, J. Chen, Z. Deng, D. Ma, Q. Li and P. Yan, A simple phosphine-oxide host with a multi-insulating structure: High triplet energy level for efficient blue electrophosphorescence, *Chem. – Eur. J.*, 2011, **17**(21), 5800–5803, DOI: 10.1002/chem.201100254.

29 J. I. Nishide, H. Nakanotani, Y. Hiraga and C. Adachi, High-efficiency white organic light-emitting diodes using thermally activated delayed fluorescence, *Appl. Phys. Lett.*, 2014, **104**(23), 1–6, DOI: 10.1063/1.4882456.

30 K. Stavrou, L. G. Franca and A. P. Monkman, Photophysics of TADF guest-host systems: introducing the idea of hosting potential, *ACS Appl. Electron. Mater.*, 2020, **2**(9), 2868–2881, DOI: 10.1021/acsaelm.0c00514.

31 P. Imbrasas, R. Lygaitis, P. Kleine, R. Scholz, C. Hänisch, S. Buchholtz, K. Ortstein, F. Talnack, S. C. B. Mannsfeld, S. Lenk and S. Reineke, Dimers or solid-state solvation? Intermolecular effects of multiple donor–acceptor thermally activated delayed fluorescence emitter determining organic light-emitting diode performance, *Adv. Opt. Mater.*, 2021, **2002153**, 1–11, DOI: 10.1002/adom.202002153.

32 S. Kumar, P. Rajamalli, D. B. Cordes, A. M. Z. Slawin and E. Zysman-Colman, Highly fluorescent emitters based on triphenylamine-π-triazine (D-π-A) System: Effect of extended conjugation on singlet-triplet energy gap, *Asian J. Org. Chem.*, 2020, **9**(9), 1277–1285, DOI: 10.1002/ajoc.202000165.
33 S. J. Su, T. Chiba, T. Takeda and J. Kido, Pyridine-containing triphenylbenzene derivatives with high electron mobility for highly efficient phosphorescent OLEDs, *Adv. Mater.*, 2008, **20**(11), 2125–2130, DOI: 10.1002/adma.200701730.
34 M. K. Etherington, N. A. Kukhta, H. F. Higginbotham, A. Danos, A. N. Bismillah, D. R. Graves, P. R. Mcgonigal, N. Haase, A. Morherr, A. S. Batsanov, P. Christof, V. Bhalla, M. R. Bryce and A. P. Monkman, Persistent dimer emission in thermally activated delayed fluorescence materials, *J. Phys. Chem. C*, 2019, **123**, 11109–11117, DOI: 10.1021/acs.jpcc.9b01458.